Control of THz Emission from Stark Wave Packets

Jeffrey L. Krause*,† and Kenneth J. Schafer‡,§

Quantum Theory Project, P.O. Box 118435, University of Florida, Gainesville, Florida 32611-8435, and Department of Physics and Astronomy, Louisiana State University, Baton Rouge, Louisiana 70803-4001

Received: June 25, 1999; In Final Form: October 7, 1999

We present calculations of the quantum control of THz emission from Stark wave packets in sodium. Our method is based on the direct integration of the one-electron, time-dependent Schrödinger equation on a non-uniform, finite difference grid. We find that simple, experimentally feasible laser pulses are sufficient to optimize the frequency and intensity of the emitted THz radiation. A genetic algorithm is used to optimize the parameters of the excitation pulse. Our results indicate that the dynamics, and hence the emitted radiation, depend sensitively on these parameters, and that the control space is rich and quite complicated.

I. Introduction

Stark wave packets are created when an atom placed in a static DC field is excited with a laser pulse.[1,2] The DC field lifts the orbital angular momentum degeneracy, and the energy levels are split by the Stark effect. For small DC fields and degenerate states, the shift is linear in the static field, and the energy levels are given by $E_{nk} = -1/2n^2 + 3/2F_snk$, where n is the principle quantum number, F_s is the magnitude of the DC field, and $k = n_1 - n_2$ is the projection of the (permanent) dipole moment of the Stark states on the axis defined by the DC field. Because the orbital angular momentum quantum number l is not conserved, the dipole selection rule $\Delta l = \pm 1$ is not obeyed, and the oscillator strength is distributed over the entire l manifold, for $l = 0, ..., n - 1$. With an appropriate laser pulse, a time-dependent superposition of Stark states is created, in which the expectation value of l oscillates from $l = 0$ to $l = n - 1$, with a period of $\tau = 2\pi/3F_sn$.

Stark wave packets have attracted attention for several reasons. First, they are manifestly quantum objects. They allow studies of time-dependent laser-matter interactions in systems that are simple enough to understand, yet display non-trivial complexity. Second, they have proven to be amenable to experimental study via a variety of methods. In particular, the evolution of Stark wave packets can be monitored by photoionization with optical pulses,[3] THz (half-cycle) pulses (HCP),[4,5] and wave-packet interferometry.[6] Recently, the HCP technique was used to deduce the entire momentum-space distribution of a Stark wave packet.[7] Finally, by modifying the form of the excitation field and the magnitude of the static DC field, Stark wave packets offer the potential to control the multi-dimensional dynamics of electrons in atoms.[8,9] Thus, Stark wave packets are prototypes for the possible control of electronic dynamics in molecules and materials. They may also be useful as reagents in chemical reactions.[10,11]

In a previous study,[9] we showed that Stark wave packets exhibit complicated, time-dependent dipole moments, and as a result should radiate in the THz frequency regime. The predicted emission spectra were shown to be extremely sensitive to the excitation conditions and the magnitude of the static field. Recent experimental work has demonstrated structure in the momentum distribution of Stark wave packets reminiscent of the dipole moments predicted in our calculations.[7] In this work we examine the extent to which the magnitude and frequency of the THz emission from Stark wave packets can be controlled. We show that simple laser pulses can be used to optimize the radiation at a desired frequency, over a broad range of frequencies. We discuss the implications of our results for future experiments, in which Stark wave packets may find application as sources of tunable, ultrafast THz radiation, or as THz detectors.

The work presented in this paper began when both authors were members of Kent Wilson's group in La Jolla, and its inspiration springs directly from Kent's dream of observing and controlling electron dynamics in molecules. We are grateful for his continued enthusiasm, insights, and encouragement.

II. Method

Several theoretical approaches to calculating the dynamics of Rydberg wave packets have been discussed in the literature. These include a variety of methods based on solutions of the time-dependent Schrödinger equation in a basis set of either hydrogenic or quantum defect wave functions, augmented by WKB (Wentzel, Kramers, and Brillouin) solutions for the continuum wave functions. For example, Alber and co-workers have used semiclassical approximations to the quantum propagator to predict recurrences and time-delayed, two-photon transition probabilities due to the periodic return of the wave packet to the ion core.[12,13] Other approaches have been pursued on a more limited basis. These include direct integration of the Schrödinger equation on a finite difference grid, for low n states,[14,15] and the use of a complex Sturmian basis to study ionization of Rydberg eigenstates in hydrogen.[16] A recent study with this method highlights the differences between experimental results on Na and calculations based on hydrogenic wave functions.[17] Reinhold et al. have studied hydrogen using a Sturmian basis set, and sodium using a classical trajectory, Monte Carlo method.[18,19]

Our approach to the dynamics of Rydberg wave packets is based upon direct numerical solutions of the time-dependent

* Corresponding author. E-mail: krause@qtp.ufl.edu.
† University of Florida.
‡ Louisiana State University.
§ E-mail: schafer@rouge.phys.lsu.edu.

10.1021/jp992144+ CCC: $18.00
Published on Web 11/10/1999

Schrödinger equation on a non-uniform finite difference grid. The grid-based method allows great flexibility in the choice of the atomic system, and a natural way to include the continuum. It also provides a practical basis for intuitive analyses and visualization of the dynamics. The methods discussed here are generalizations of the uniform grid methods reviewed in Kulander et al.,[20] which have been used to study such intense-field phenomena as above-threshold ionization,[21] high-order harmonic generation,[22] and high-frequency stabilization.[23]

The method begins with the time-dependent Schrödinger equation for a one-electron atom interacting with a coherent laser field $\vec{\epsilon}(t)$ in the presence of a static DC field, F_s. This equation can be written in the length-gauge as

$$i\dot{\psi}(r,t) = [H_0 + F_s z + \vec{\epsilon}(t)\cdot\vec{r}]\psi(r,t) \tag{1}$$

where H_0 is the (field-free) one-electron Hamiltonian. We assume that the laser polarization is parallel to the applied DC field, which means that the total Hamiltonian has azimuthal symmetry and the magnetic quantum number, m, is conserved. For simplicity, we assume $m = 0$ throughout, and suppress the m label in the following equations. Atomic units ($\hbar = e = m_e = 1$) are used throughout.

The wave function $\psi(r,t)$ is expanded in a mixed basis of discretized radial functions and spherical harmonics. Although it is certainly possible to use other coordinate systems, spherical coordinates offer a simple way to treat non-hydrogenic atoms by using l-dependent pseudopotentials of the form[24,25]

$$V_{\text{pseudo}}(\vec{r}) = \sum_l V_l(r)|l\rangle\langle l| - 1/r \tag{2}$$

where $V_l(r)$ contains only short-range interactions. There is no additional computational labor associated with using such potentials as compared to solving the pure Coulomb problem, and excellent pseudopotentials are available for the alkali metal atoms.[26]

We solve the full atom plus DC field plus laser problem by first computing a basis of eigenstates, $|k\rangle$, of the Stark Hamiltonian, $H^s|k\rangle = E_k|k\rangle$, where $H^s = H_0 + F_s z$. This is accomplished by diagonalizing H^s in a finite subspace of the field-free Hamiltonian H_0. The calculation of the field-free basis states is discussed in detail in the Appendix. The main technical innovation employed in this work is the use of a non-uniform finite difference grid. The radial grid is very fine near the ion core and becomes progressively coarser away from the $r = 0$ boundary. A useful parameterization of the grid is in terms of three parameters, $\Delta_{\min}$, $\Delta_{\max}$, and α where

$$r_j = r_{j-1} + \Delta_{\min} + (1 - e^{-\alpha r_{j-1}})(\Delta_{\max} - \Delta_{\min}) \tag{3}$$

with the convention that the first grid point is located at $+\Delta_{\min}/2$. The grid spacing varies smoothly from a $\Delta_{\min}$ to $\Delta_{\max}$. For the calculations presented here, we typically use $\Delta_{\min} = 0.01$ au, $\Delta_{\max} = 5$ to 10 au, and $\alpha \approx 0.002$. This creates a computational "box" of size $O(10^4)$ au, meaning that up to $n \approx 100$ bound states can be determined accurately for each l value using $O(10^3)$ radial grid points. The radial basis states, $\phi_l^n(r)$, satisfy $H_l^0\phi_l^n = E_{nl}\phi_l^n$ and have definite angular momentum l. The Stark eigenstates $|k\rangle$ are calculated as linear combinations of the field-free eigenfunctions,

$$|k\rangle = \sum_l \sum_{n_{\min}}^{n_{\max}} b_{nl}^k \phi_l^n(r)|l\rangle = \sum_l \phi_l^k(r)|l\rangle \tag{4}$$

where the coefficients b_{nl}^k are obtained by diagonalizing a sparse banded matrix. The eigenstates $|k\rangle$ do not have definite angular momentum, as noted above.

The total number N of basis states required in a given calculations is dictated by $n_{\min}$ and $n_{\max}$, the lowest and highest Stark manifolds that are included in the diagonalization of the Hamiltonian. Defining $\bar{n} = (n_{\max} + n_{\min})/2$ and $\Delta n = n_{\max} - n_{\min} + 1$, the total number of basis states is $N = \bar{n}\Delta n$. As $\bar{n}$ increases, it is desirable to maintain the energy ΔE spanned by the finite subspace as approximately constant. Due to the compression of the Rydberg states in energy, this requires including additional manifolds in the diagonalization. Qualitatively, to lowest order in $\Delta n/\bar{n}$,

$$\Delta E \approx 4E_{\bar{n}}\frac{\Delta n}{\bar{n}} \tag{5}$$

This equation implies that as $\bar{n}$ increases, holding ΔE constant requires $\Delta n \propto \bar{n}$, and thus N scales as $\bar{n}^2$.

Solving eq 1 proceeds by expanding the full time-dependent wave function $\psi(t)$ in eigenstates of H^s,

$$\psi(r,t) = \sum_k C_k(t)|k\rangle \tag{6}$$

In the weak field limit, the promoted wave packet is defined as

$$|\psi^0(t)\rangle = e^{-i(H^s - E_0 - \omega_L)t}\hat{\mu}\cdot\vec{r}\,|0\rangle \tag{7}$$

where $\hat{\mu}$ is the laser polarization direction, and ω_L is the center frequency of the laser. The time-dependent wave packet (within the usual rotating wave approximation and first-order perturbation theory) is

$$|\psi_{\text{wp}}(t)\rangle = \int_0^{t-t_0} d\tau\epsilon(t-\tau)|\psi^0(\tau)\rangle \tag{8}$$

where t_0 is a time well before the beginning of the laser pulse. Under these approximations, the expansion coefficients in eq 6 are

$$C_k(t) = \int_0^{t-t_0} d\tau\epsilon(t-\tau)e^{-i\omega_k\tau}\langle k|z|0\rangle \tag{9}$$

In this equation, $\epsilon(t)$ is the (complex) envelope of the laser field and $\omega_k = E_k - E_0 - \omega_L = \omega_{k0} - \bar{\omega}$, where $\bar{\omega}$ is the center frequency of the excitation. The transition moment, $\Omega_{k0} = \langle k|z|0\rangle$, connects the initial state, with a definite angular momentum L, to the $L \pm 1$ components of the various $|k\rangle$ states. Since l is not a good quantum number, all of the $|l\rangle$ states are populated rapidly by the field. The transition moments depend on the initial state and the static field. They must be recalculated if either quantity is changed. To be explicit, if the initial state is $|0\rangle = \Phi(r)|L\rangle$ then

$$\Omega_{k0} = a_L\int \mathrm{d}r\phi_{L+1}^k(r)r\Phi(r) + a_{L-1}\int \mathrm{d}r\phi_{L-1}^k(r)r\Phi(r) \tag{10}$$

where

$$a_l = \frac{l+1}{\sqrt{(2l+1)(2l+3)}} \tag{11}$$

There are slight modifications to these equations if m is not, as assumed here, equal to zero. The radial integrals can be calculated rapidly as simple summations over the finite difference grid.

Once the excitation pulse is over (at time t_p) the propagation of the wave packet can be performed by multiplication by an

appropriate phase,

$$|\psi_{\mathrm{wp}}(t \geq t_p)\rangle = \sum_k C_k(t_p) e^{-i\omega_k(t-t_p)} |k\rangle \tag{12}$$

In the weak-field limit the coefficients $C_k(t_p)$ are then

$$C_k(t_p) = \tilde{\epsilon}(\omega_k)\Omega_{k0} \tag{13}$$

where $\tilde{\epsilon}(\omega_k)$ is the complex Fourier coefficient of the field at the frequency $\omega_k = E_k - \bar{E}$. This equation illustrates explicitly that in the limit discussed here, the phase of the laser field is transformed directly to the phase of the wave function of the electron.

After the basis states, $|k\rangle$, transition moments, Ω_{k0}, and coefficients, $C_k(t)$, have been calculated and stored, a variety of quantities of interest can be calculated. Defining the following matrices:

$$R_{k,k'} = \langle k|r|k'\rangle = \sum_l \int \mathrm{d}r\, r^2 \phi_l^k(r) r \phi_l^{k'}(r) \tag{14}$$

$$Z_{k,k'} = \langle k|z|k'\rangle = \sum_l \int \mathrm{d}r\, r^2 \phi_l^k r [a_l\, \phi_{l+1}^{k'} + a_{l-1}\phi_{l-1}^{k'}] \tag{15}$$

and

$$L_{k,k'}^2 = \sum_l l\,(l+1) \int \mathrm{d}r\, r^2 \phi_l^k(r) \phi_l^{k'}(r) \tag{16}$$

allows facile calculation of expectation values such as

$$\langle r\rangle(t) = \sum_{k,k'} C_k^*(t) C_{k'}(t) R_{k,k'} \tag{17}$$

$$\langle L^2\rangle(t) = \sum_{k,k'} C_k^*(t) C_{k'}(t) L_{k,k'}^2 \tag{18}$$

and

$$\langle z\rangle(t) = \sum_{k,k'} C_k^*(t) C_{k'}(t) Z_{k,k'} \tag{19}$$

which are all double sums over the (few hundred) Stark coefficients.

The acceleration form of the time-dependent dipole moment can be calculated from the double commutator of the Hamiltonian as

$$\frac{\mathrm{d}^2}{\mathrm{d}t^2}\langle z\rangle(t) = \langle \psi_{\mathrm{wp}}|[H,[H,z]]|\psi_{\mathrm{wp}}\rangle \tag{20}$$

After the laser pulse is over, the Stark states are eigenstates of the Hamiltonian, and eq 20 simplifies to

$$\frac{\mathrm{d}^2}{\mathrm{d}t^2}\langle z\rangle(t > t_p) = \sum_{k,k'} C_k^*(t) C_{k'}(t) Z_{k,k'} (\omega_{k,k'})^2 \tag{21}$$

where $\omega_{k,k'} = \omega_k - \omega_{k'}$.

III. Calculation of THz Emission

As can be seen in the preceding section, a variety of expectation values can be calculated readily for Stark wave packets, all of which are potential candidates for control. In this work we choose to concentrate on the photon emission resulting from the time-dependent dipole moment induced in the atom by the excitation pulse. Figure 1 shows two snapshots of a Stark wave packet created by a short (275 fs) laser pulse centered near the middle of the $n = 15$ manifold in sodium. As can be seen in the figure, the wave packet is quite complicated, and the electronic distribution is highly asymmetrical, with a rapidly varying dipole moment.

The acceleration form of the spectrum is the Fourier transform of $\ddot{z}$:

$$A(\omega) = \frac{1}{T}\int_{t_0}^{t_0+T} \mathrm{d}t\, e^{i\omega t}\, \ddot{z}(t) \tag{22}$$

with z defined in eq 19. The signal (number of photons) at a detector is proportional to $|A(\omega)|^2$ times the integration time:[27]

$$S(\omega) \propto T|A(\omega)|^2 \tag{23}$$

One possible control scenario involving photon emission is to optimize the spectral intensity in a band of frequencies centered around a selected center frequency ω. At times after the excitation pulse is over the spectrum is

$$A(\omega) = \sum_{k,k'} C_k^*(t_p) C_{k'}(t_p) Z_{k,k'} (\omega_{k,k'})^2 \delta(\omega, \omega_{k,k'}) \tag{24}$$

Barring an accidental coincidence, the delta function picks out a single set of states separated by ω. Since the number of states is in general huge, and the Stark manifolds split linearly (at low DC field), there is a high probability that two or more sets of states will have nearly the same frequency differences. Therefore, we choose a minimum difference between two sets of states (i.e., a frequency bin) and add the contributions inside the bin coherently.

Assuming that all of the frequency differences are distinct, the spectral intensity can be written as

$$|A(\omega_{k,k'})|^2 = P_k P_{k'} Z_{k,k'}^2 (\omega_{k,k'})^4 \tag{25}$$

where $P_k = |C_k|^2$. This equation shows that the spectral intensity is proportional to the product of the population in the two states separated by $\omega_{k,k'} = \omega$, the square of the dipole matrix element connecting the two states, and the fourth power of the frequency difference. Notice, however, that the spectral intensity is independent of the *phase* of the population amplitudes. Thus, chirping, or otherwise altering the time-dependent phase of the excitation pulse cannot increase or decrease the total number of photons in a particular frequency bin (at least within first-order perturbation theory).

In the weak field limit the expression for the frequency spectra can be written as

$$|A(\omega_{k,k'})|^2 = |\tilde{\epsilon}(\omega_k)|^2 \Omega_{k0}^2 |\tilde{\epsilon}(\omega_{k'})|^2 \Omega_{k'0}^2 Z_{k,k'}^2 (\omega_{k,k'})^4 \tag{26}$$

If the pulse envelope is defined as

$$\epsilon(t) \propto e^{-2\ln 2 t^2/\tau^2} \tag{27}$$

where τ is the FWHM in intensity, the corresponding quantity in the frequency domain is

$$|\tilde{\epsilon}(\omega)|^2 \propto e^{-4\ln 2(\omega-\bar{\omega})^2/\Delta\omega^2} \tag{28}$$

where $\bar{\omega}$ is the central frequency and $\Delta\omega = 4\ln 2/\tau$ is the

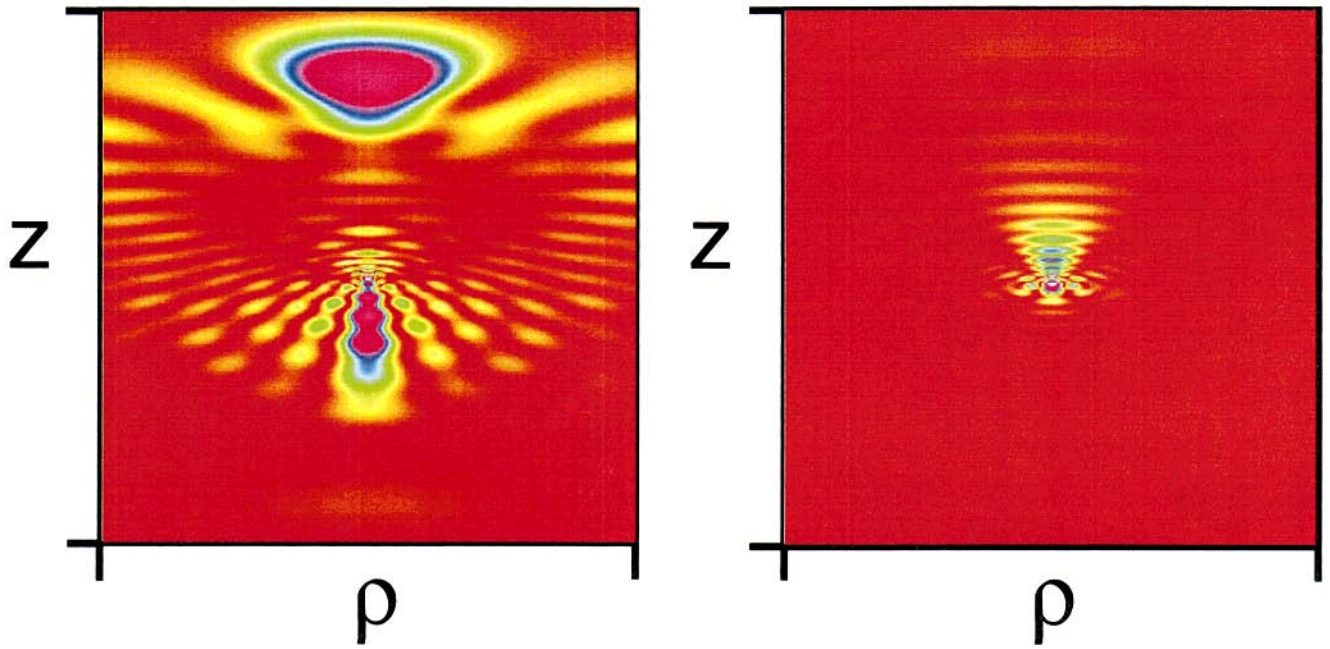

Figure 1. Two snapshots of the probability distribution for the electron in a Stark wave packet in sodium. The initial state is the 3d state, and the static DC field is 400 V/cm. The center frequency of the laser is 1.47 eV, with a pulse width of 275 fs. The left panel shows the wave packet after 12 ps, and the right panel after 40 ps. The ρ axis ranges from −150 au (−7.9 nm) to 150 au (7.9 nm), and the z axis ranges from −450 au (−24 nm) to 450 au (24 nm).

frequency bandwidth. Using these expressions, eq 26 simplifies to

$$|A(\omega_{k,k'})|^2 \propto [\omega_{k,k} e^{-\ln 2\omega^2_{k,k'}/\Delta\omega^2}]^4 \, e^{-4\ln 2\omega_k\omega_{k'}/\Delta\omega^2} \Omega^2_{k0}\Omega^2_{k'0}Z^2_{k,k'} \tag{29}$$

where $\omega_k = \omega_{k0} - \bar{\omega}$.

In eq 29, the expression in brackets has a maximum when $\omega_{k,k'} \approx .85\Delta\omega$. The second exponential is maximized if either ω_k or $\omega_{k'}$ is close to zero, i.e., if one or the other state is near the central frequency of the excitation laser. This formula suggests that the optimal signal can be obtained by exciting two states, such that one is near the central frequency, and the other is well off-resonance. However, as illustrated previously, the situation is far more complex and non-intuitive than this simple analysis suggests. In particular, the transition moments have pronounced energy dependencies (because of the differing angular momentum content of the various states) and the matrix elements $Z_{k,k'}$, which scale as n^2, vary from zero to very large numbers. In our previous work we presented an example in which the THz signal had a dominant component at 30 cm^{-1} even though the bandwidth of the laser was only 6 cm^{-1}. In that case one state had $\omega_k \approx 0$ and the other state was about $5\Delta\omega$ away in energy. However, both states had relatively large transition moments and the dipole element $Z_{k,k'}$ was enormous ($Z^2_{k,k'} \approx 15\,000$; the matrix elements $Z^2_{k,k'}$ as a function of $\omega_{k,k'}$ varied over 7 orders in magnitude in that example).

IV. Results

In the preceding section we sketched the derivation of some simple formulas to determine the frequency spectrum of THz emission from Stark states. Optimizing this emission, however, is not as simple, for two main reasons. The first is that there are a huge number of states, all of which are connected via dipole moments. This means that there are many possible sources for emission at a given frequency. The second is that the amplitudes of the dipole moments vary over many orders of magnitude, which implies that simply searching for a pair of states with the proper energy difference will not guarantee that that particular pair of states will contribute to the spectrum significantly.

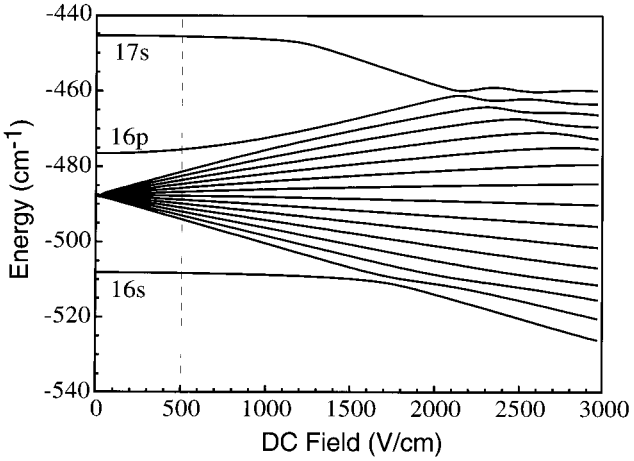

Figure 2. A portion of the $n = 15$ Stark manifold in sodium.

For concreteness, let us consider a specific example. Figure 2 shows a portion of the $n = 15$ Stark manifold of sodium. Most of the calculations presented here are for DC fields of ∼500 V/cm, which, as seen in the figure, corresponds to a regime in which the 16s and 16p states are split off from the manifold, and the remaining $|k\rangle$ states are split linearly with the DC field.

Figure 3 shows the square of the dipole transition moment $\Omega_{k'0}$, and the expectation value of the distance of the electron from the nucleus, $\langle z \rangle$, again for the $n = 15$ manifold of sodium. For this figure, the static DC field was set to 500 V/cm, and the atom was assumed to be initially in the 3d state. The bandwidth of the excitation laser was ≈12 cm^{-1}, and the center frequency $E_0 + \omega_L = -480$ cm^{-1}, which placed it midway

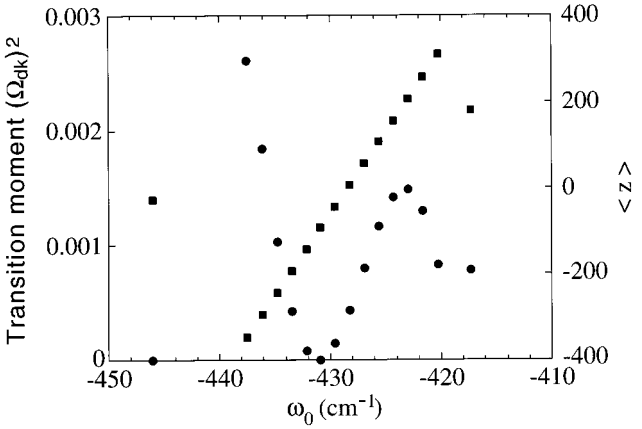

Figure 3. Square of the dipole moment (filled squares) and expectation value of z (filled circles) for a Stark wave packet in sodium. The initial state is the 3d state, and the static DC field is 400 V/cm. The center frequency of the laser is $E_0 + \omega_L = -480$ cm^{-1}, with a pulse width of 1 ps.

between the $n = 15$ and $n = 16$ Stark manifolds. The figure shows, as expected from Figure 2, that fourteen of the sixteen Stark states are split linearly in z. However, the distribution of transition moments is much more complicated. The matrix element to the 16s state is equal to zero, because at this value of the static field the 16s state does not mix with the other members of the manifold, and so the $\Delta l = \pm 1$ selection rule is (nearly) obeyed. Notice, though, that the matrix element to the 7th Stark state is also (accidentally) nearly equal to zero, and that the overall pattern is quite complex, with considerable, non-intuitive structure.

As Figure 3 suggests, the THz spectrum is a complicated function of the parameters of the excitation pulse and the strength of the static field. One approach to optimizing the emission is to use formal control theory to determine the optimal laser fields.[28−31] The difficulty with this approach is that most existing methods assume a quadratic control functional. The THz signal, which is proportional to the second derivative of the time-dependent dipole moment, cannot be expressed in quadratic form. Our solution to this problem is to use an alternative control procedure, in which a functional minimization routine is used to search for the optimal laser parameters (eq 28) and the static DC field strength. We note that other, more elaborate, pulse-shaping schemes are certainly possible, especially with current laser technology. However, for the targets considered below, only two laser parameters are important, the excitation frequency, $\bar{\omega}$, and the bandwidth, $\Delta\omega$.

The minimization routine used in this work is a genetic algorithm (GA) that uses the standard genetic operators of crossover and mutation.[32] We find that this method is quite efficient, and converges rapidly to the optimal parameters, typically after several hundred evaluations of the test function. Other minimization algorithms can also be employed, which may have advantages in certain cases. Particularly interesting in this regard are evolution algorithms,[33] which use the same basic genetic operators as the GA, but apply them with different precedence. In addition, some parameters of EAs are determined adaptively during the optimization, which may be responsible for some of their success in recent experimental implementations.[34]

Figure 4 shows the results of optimizing the THz emission via excitation to near the center of the $n = 15$ Stark manifold in sodium, at a fixed DC field of 500 V/cm. In this case we chose to optimize the emission in a 1 cm^{-1} frequency bin at

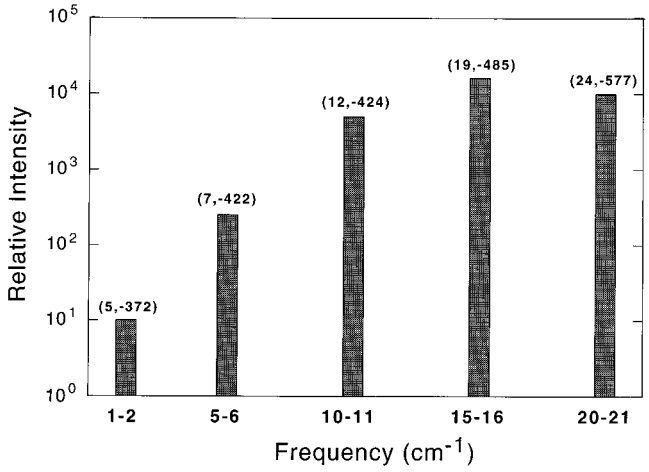

Figure 4. Optimization of the bandwidth and center frequency for a set of 1 cm^{-1} bins. The height of the bars shows the relative magnitude of the emission. The numbers in parentheses above the bars indicate the bandwidth (in cm^{-1}) and the center frequency (in cm^{-1}), respectively, of the excitation pulse. The magnitude of the static DC field is 500 V/cm. The initial state is the 3d state. In this figure, "center frequency" refers to the frequency at which the excitation occurs.

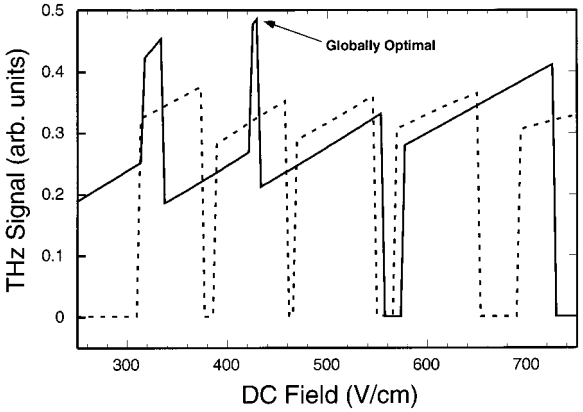

Figure 5. Variation of the THz emission in a bin of 15−16 cm^{-1} with the static DC field. The dashed line shows the magnitude of the signal using the optimal bandwidth (19 cm^{-1}) and center frequency (−485 cm^{-1}) at 500 V/cm. The solid line shows the results when all three parameters are allowed to vary. The globally optimal point occurs at a bandwidth of 17.1 cm^{-1}, a center frequency of −553 cm^{-1}, and a DC field of 426 V/cm. The initial state is the 3d state. In this figure, "center frequency" refers to the frequency at which the excitation occurs.

five different frequencies. The figure indicates that as the desired THz frequency increases, the optimal bandwidth also increases. This is sensible because the larger the bandwidth, the more likely it is that two states within the bandwidth of the excitation pulse have a frequency difference equal to the desired emission frequency. However, since the contributions are added coherently, and since the system is often dominated by a single transition, the optimal solution is *not* simply to increase the bandwidth to as large a value as possible (if the total energy per pulse is kept constant, as it is in these calculations). Notice also in Figure 4 that the center frequency increases as the desired THz frequency increases. There is no particular reason to expect this behavior a priori.

The results in Figure 4 give a hint of the extreme sensitivity of the THz emission to the parameters of the excitation pulse. However, the magnitude of the emission also depends on the DC field. Figure 5 shows the dependence of the THz emission in a frequency bin of 15−16 cm^{-1}, as a function of the

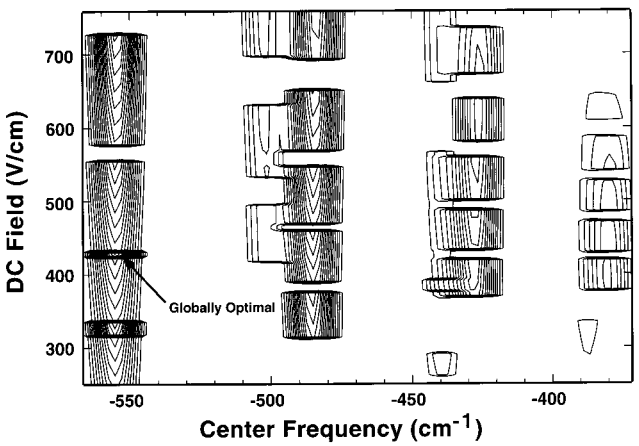

Figure 6. Control map showing the variation of the THz emission with respect to the center frequency and the static DC field. The bandwidth of the excitation laser is fixed at 17.1 cm^{-1}. The initial state is the 3d state. In this figure, "center frequency" refers to the frequency at which the excitation occurs.

magnitude of the DC field. The figure contains two traces. In one, the parameters of the laser field are held at their optimal values for a field of 500 V/cm. In the other, all three parameters are allowed to vary. As the figure illustrates, allowing the DC field to vary increases the maximum THz emission by nearly a factor of two. Finally, Figure 6 shows a control map of the DC field versus the center frequency, with the bandwidth at its optimal value. The basin of attraction for the globally optimal solution is seen to be rather narrow, and well-localized in parameter space. This would make it nearly impossible to locate with low-level search methods such as conjugate gradient, or by simply guessing.

V. Conclusions

In this paper we have investigated one aspect of the optimization of THz emission from Stark wave packets. In particular, we have shown that the magnitude of the emission is extremely sensitive to the excitation conditions and the static field, and that the parameters can be optimized with the aid of a genetic algorithm. Of course, optimizing the magnitude of the photon emission in a narrow frequency bin is only one of many possible control scenarios. Other possibilities include producing optimal trains of pulses, or coherently related bursts of radiation that might be then compressed to form ultrashort pulses, or used in spectroscopy. It may also be possible to optimize additional expectation values to create, for example, squeezed Stark wave packets, or wave packets localized in both l and r.

Finally, it is intriguing, and certainly Wilsonian in spirit, to speculate about the prospects of performing similar analyses in polyelectron atoms and molecules. The one-electron Stark wave packets discussed here display a remarkable range of complexity. Systems with more electrons will be considerably more complex, which will make them even more difficult to analyze. At the same time, the vast number of states, and intricate couplings will offer potential applications in a wide variety of control scenarios.

VI. Acknowledgments

Acknowledgment is made by J.L.K. to the Donors of The Petroleum Research Fund, administered by the American Chemical Society, for partial support of this research. This work was partially supported by the National Science Foundation through Grant CHE-9875080. J.L.K. is a Cottrell Scholar of the Research Corporation. K.J.S. acknowledges support by the Louisiana State Board of Regents through Grant LEQSF96-99-Rd-A-14.

Appendix: Derivation of Non-Uniform Grid Equations

In this appendix we present the method that we have developed to solve a discretized version of the Schrödinger equation on a non-uniform finite-difference grid. We begin with methods presented previously for uniform grids.[20,35] The action is defined as

$$S = \int_{t_1}^{t_2} \mathrm{d}t\, L(\psi,\psi^*) \tag{A1}$$

where the Lagrangian is

$$L = \left\langle \psi \middle| i\frac{\partial}{\partial t} - T - V \middle| \psi \right\rangle \tag{A2}$$

Variation of the action with respect to ψ^*, $\delta S/\delta\psi^* = 0$, for fixed t_1 and t_2, yields an equation of motion for ψ. Note that this is equivalent to requiring that ψ^* obey the Euler−Lagrange condition

$$\frac{\mathrm{d}}{\mathrm{d}t}\left(\frac{\partial L}{\partial \dot{\psi}^*}\right) - \frac{\partial L}{\partial \psi^*} = 0 \tag{A3}$$

For a continuous wave function, this procedure leads directly to a formulation of the time-dependent Schrödinger equation (TDSE) for ψ. For a discretized wave function, the procedure leads to a discretized version of the TDSE that efficiently accounts for the boundary conditions imposed on ψ, especially at small r.

The static (atomic) potentials used in this work are of the form

$$V(\vec{r}) = U(r) + \sum_l V_l(r)|l\rangle\langle l| \tag{A4}$$

where $U(r)$ is a spherically symmetric potential (containing Coulomb and possibly polarization terms) and $V_l(r)$ are angular-momentum-dependent, short-range pseudopotentials for the atomic system. The centrifugal term $l(l+1)/2r^2$ is included in V_l, so T refers to the radial kinetic energy only.

The wave function is expanded in a mixed basis consisting of a product of discretized radial functions and spherical harmonics,

$$\psi(r_j,\theta,\phi,t) = \sum_{l,m}^{l_{\max}} \phi_{lm}(r_j,t) Y_l^m(\theta,\phi) \tag{A5}$$

To simplify the notation, we assume that the potential is cylindrically symmetric, which means that the m quantum number is conserved. For this reason, the label m is suppressed in the following equations. The one-dimensional space $r_{min} = 0$ to $r_{max} = R$ is divided into N intervals with knots at $r_j\{j = 1...N\}$, which are not required to be evenly spaced. The wave function is known at these points only. We assume that $\phi_l(R) = 0$, $r\phi_l(r) = 0$, and $r\partial\phi_l/\partial r = 0$ at $r = 0$. With these boundary conditions, the equations of motions can be derived for the coefficients $\phi_l^j \equiv \phi_l(r_j,t)$.

To proceed, we must first define approximate integration schemes for the integrals in the Lagrangian. This determines the particular finite difference scheme that we use. After integrating over the angular variables the remaining integrals

in L are discretized as

$$\left\langle i\frac{\partial}{\partial t}\right\rangle = \sum_{l=0}^{l_{max}}\int_0^R dr\, r^2\phi_l^*\, i\frac{\partial\phi_l}{\partial t} \approx \sum_{l=0}^{l_{max}}\sum_{j=1}^{N}\left[\frac{r_{j+1}-r_{j-1}}{2}\right] r_j^2(\phi_l^j)^* i\frac{\partial\phi_l^j}{\partial t} \tag{A6}$$

$$\langle T\rangle = \frac{1}{2}\sum_{l=0}^{l_{max}}\int_0^R dr\, r^2\left|\frac{\partial\phi_l}{\partial r}\right|^2 \approx \frac{1}{2}\sum_{l=0}^{l_{max}}\sum_{j=1}^{N}(r_{j+1}-r_j)\left[\frac{r_{j+1}+r_j}{2}\right]^2\left|\frac{\phi_l^{j+1}-\phi_l^j}{r_{j+1}-r_j}\right|^2 \tag{A7}$$

and

$$\langle V\rangle = \sum_{l=0}^{l_{max}}\int_0^R dr\, r^2\phi_l^*(U(r)+V_l(r))\phi_l \approx \sum_{l=0}^{l_{max}}\sum_{j=1}^{N}\left[\frac{r_{j+1}-r_{j-1}}{2}\right] r_j^2(\phi_l^j)^*(U^j+V_l^j)\phi_l^j \tag{A8}$$

As can be seen in these expressions, the derivative term is evaluated at the mid point of each interval, using the *local* grid spacing as an integration weight, and the potential term is evaluated on the grid points, using the *average* of the local grid spacing on each side of the knot as the integration weight.

Substituting these expressions into L and shifting indices on the radial summations in accord with the boundary conditions stated above leads to

$$L = \sum_{l=0}^{l_{max}}\sum_{j=1}^{N}(\phi_l^j)^*\left\{\frac{r_{j+1}-r_{j-1}}{2} r_j^2\, i\frac{\partial\phi_l^j}{\partial t} - \frac{1}{2}\left[\frac{\phi_l^j-\phi_l^{j-1}}{r_j-r_{j-1}}\left[\frac{r_j+r_{j-1}}{2}\right]^2 - \frac{\phi_l^{j+1}-\phi_l^j}{r_{j+1}-r_j}\left[\frac{r_{j+1}+r_j}{2}\right]^2\right] - \frac{r_{j+1}-r_{j-1}}{2} r_j^2(U^j+V_l^j)\phi_l^j\right\} \tag{A9}$$

We next transform to the normalized coefficients g_j^l, which are related to ϕ_l^j by

$$g_l^j = r_j\sqrt{\frac{r_{j+1}-r_{j-1}}{2}}\phi_l^j \tag{A10}$$

Since the wave function $\psi(\vec{r},t)$ is normalized, it follows that

$$\sum_{l=0}^{l_{max}}\sum_{j=1}^{N}|g_l^j|^2 = 1 \tag{A11}$$

Imposing the Euler−Lagrange condition with respect to $(g_l^j)^*$, we arrive at an equation for the time evolution of g_l^j. This equation is

$$i\frac{\partial g_l^j}{\partial t} = [\tilde{H}_0\, g]_l^j = -\frac{1}{2}[c_j g_l^{j+1} - 2d_j g_l^j + c_{j-1}g_l^{j-1}] + (U^j+V_l^j)g_l^j \tag{A12}$$

where the coefficients c_j and d_j are

$$c_j = \frac{2}{r_{j+1}-r_j}\sqrt{\frac{1}{(r_{j+2}-r_j)(r_{j+1}-r_{j-1})r_{j+1}r_j}}\left[\frac{r_{j+1}+r_j}{2}\right]^2 \tag{A13}$$

and

$$d_j = \frac{1}{r_{j+1}-r_{j-1}}\left\{\frac{1}{r_j-r_{j-1}}\left[\frac{r_j+r_{j-1}}{2r_j}\right]^2 + \frac{1}{r_{j+1}-r_j}\left[\frac{r_{j+1}+r_j}{2r_j}\right]^2\right\} \tag{A14}$$

Here, $\tilde{H}_0$ is the field-free Hamiltonian matrix, which is block-diagonal in the l quantum number and tridiagonal in the radial index. Note that for a uniform grid spacing, Δ, far from the $r = 0$ boundary, both c_j and d_j, as defined above, approach the value $1/\Delta^2$, and the standard second-order finite-difference equations are recovered.

To obtain the field-free basis states used in our calculations we diagonalize separately a symmetric tridiagonal matrix $\tilde{H}_0^l$ for each angular momentum value. Since we require only the lowest few hundred states, this diagonalization can be performed in $O(N)$ operations, where N is the number of radial grid points.

References and Notes

(1) Gallagher, T. F. *Rydberg Atoms*; Cambridge University Press: Cambridge, 1994.

(2) Jones, R. R.; Noordam, L. D. *Adv. At. Mol. Opt. Phys.* **1997**, *38*, 1−37.

(3) Noordam, L. D.; ten Wolde, A.; Lagendijk, A.; van Linden van den Heuvell, H. B. *Phys. Rev. A* **1989**, *40*, 6999−7006.

(4) Raman, C.; Weinacht, T. C.; Bucksbaum, P. H. *Phys. Rev. A* **1997**, *55*, R3995−R3998.

(5) Frey, M. T.; Dunning, F. B.; Reinhold, C. O.; Burgdörfer, J. *Phys. Rev. A* **1997**, *55*, R865−R868.

(6) Naudeau, M. L.; Sukenik, C. I.; Bucksbaum, P. H. *Phys. Rev. A* **1997**, *56*, 636−639.

(7) Campbell, M. B.; Bensky, T. J.; Jones, R. R. *Phys. Rev. A* **1999**, *59*, R4117−4120.

(8) Krause, J. L.; Wilson, K. R.; Yan, Y. J. Quantum control of electron dynamics. In *Laser Techniques for State-Selected Chemistry II*; Hepburn, J. W., Ed.; SPIE: Bellingham, WA, 1994.

(9) Schafer, K. J.; Krause, J. L. *Opt. Express* **1997**, *1*, 210−215.

(10) Nordlander, P.; Dunning, F. B. *Nucl. Instrum. Meth. B* **1997**, *125*, 300−304.

(11) Bensky, T. J.; Campbell, M. B.; Jones, J. J. *Phys. Rev. Lett.* **1998**, *81*, 3112−3115.

(12) Alber, G.; Ritsch, H.; Zoller, P. *Phys. Rev. A* **1986**, *34*, 1058−1064.

(13) Alber, G.; Zoller, P. *Phys. Rep.* **1991**, *199*, 231−279.

(14) LaGattuta, K. J.; Lerner, P. B. *Phys. Rev. A* **1994**, *49*, R1547−1550.

(15) LaGattuta, K. J. *Phys. Rev. A* **1996**, *53*, 1762−1766.

(16) Bugacov, A.; Piraux, B.; Pont, M.; Shakeshaft, R. *Phys. Rev. A* **1995**, *51*, 1490−1494.

(17) Bugacov, A.; Piraux, B.; Pont, M.; Shakeshaft, R. *Phys. Rev. A* **1995**, *51*, 4877−4880.

(18) Reinhold, C. O.; Melles, M.; Shao, H.; Burgdörfer, J. *J. Phys. B* **1993**, *26*, L659−L664.

(19) Reinhold, C. O.; Burgdörfer, J.; Jones, R. R.; Raman, C.; Bucksbaum, P. H. *J. Phys. B* **1995**, *28*, L457−L464.

(20) Kulander, K. C.; Schafer, K. J.; Krause, J. L. Time-dependent studies of multiphoton processes. In *Atoms in Intense Radiation Fields*; Gavrila, M., Ed.; Academic Press: New York, 1992.

(21) Schafer, K. J.; Kulander, K. C. *Phys. Rev. A* **1992**, *45*, 8026−8033.

(22) Krause, J. L.; Schafer, K. J.; Kulander, K. C. *Phys. Rev. Lett.* **1992**, *68*, 3535−3538.

(23) Kulander, K. C.; Schafer, K. J.; Krause, J. L. *Phys. Rev. Lett.* **1991**, *66*, 2601−2604.

(24) Bardsley, J. N.; Junker, B. R.; Norcross, D. W. *Chem. Phys. Lett.* **1976**, *37*, 502−506.

(25) Kulander, K. C.; Rescigno, T. N. *Comput. Phys. Commun.* **1991**, *63*, 523−528.

(26) Bardsley, J. N. Pseudopotentials in atomic and molecular physics. In *Case Studies in Atomic Physics, Vol. 4*; McDaniel, E. W., McDowell, M. R. C., Eds.; North Holland: Amsterdam, 1975.

(27) Milonni, P. W.; Eberly, J. H. *Lasers*; Wiley: New York, 1988.

(28) Tannor, D. J.; Rice, S. A. *Adv. Chem. Phys.* **1988**, *70*, 441−524.

(29) Shapiro, M.; Brumer, P. *Int. Rev. Phys. Chem.* **1994**, *13*, 187−229.

(30) Neuhauser, D.; Rabitz, H. *Acc. Chem. Res.* **1993**, *26*, 496−501.
(31) Krause, J. L.; Whitnell, R. M.; Wilson, K. R.; Yan, Y. J. Light packet control of wave packet dynamics. In *Femtosecond Chemistry*; Manz, J., Wöste, L., Eds.; VCH: Weinheim, 1995.
(32) Grefenstette, J. D. *GENESIS*, version 5.0; 1990.
(33) Schwefel, H.-P. *Evolution and optimum seeking*; Wiley: New York, 1995.
(34) Assion, A.; Baumert, T.; Bergt, M.; Brixner, T.; Kiefer, B.; Seyfried, V.; Strehle, M.; Gerber, G. *Science* **1998**, *282*, 919−922.
(35) Negle, J. W. *Rev. Mod. Phys.* **1982**, *54*, 913−1015.